

Electronic Supplementary Information for
Pre-phase transition of Cu_{2-x}S template enables
polymorph selective synthesis of MS (M = Zn, Cd,
Mn) nanocrystals via cation exchange reactions

Yan Zhang,^{a,d} Shaobo He,^a Qingxia Zhang,^a Hongtao Zhang,^a Jinchen Zhou,^a Xing Yang,^a
Qinhong Wei,^a Lihui Chen^{*a,b,c}

^a*School of Petrochemical Engineering & Environment, Zhejiang Ocean University, No.1,
Haida South Road, Lincheng Changzhi Island, Zhoushan 316022, China*

^b*Zhejiang Key Laboratory of Petrochemical Environmental Pollution Control, Zhoushan
316022, China*

^c*National & local Joint Engineering Research Center of Harbor Oil & Gas Storage and
Transportation Technology, Zhoushan 316022, China*

^d*School of Naval Architecture and Maritime, Zhejiang Ocean University, No.1, Haida South
Road, Lincheng Changzhi Island, Zhoushan 316022, China*

Chemicals and Materials

Copper(I) chloride (CuCl , $\geq 99.95\%$), cadmium(II) chloride hemi(pentahydrate) ($\text{CdCl}_2 \cdot 2.5\text{H}_2\text{O}$, 99.95%), zinc(II) chloride (ZnCl_2 , 99.95%), manganese(II) chloride tetrahydrate ($\text{MnCl}_2 \cdot 4\text{H}_2\text{O}$, 99.99%), 1-octadecene (ODE, $>90.0\%$), oleylamine (OAm, $80\text{--}90\%$), cyclooctasulfur (S_8), 1-dodecanethiol (1-DDT, 98%), trioctyl-phosphine (TOP, 90%), ethanol (99.5%), hexane (97%), toluene, acetone, chloroform (CHCl_3) and other chemicals were purchased from Aladdin Chemicals. All the chemicals were used as received without further purification.

Characterizations

TEM observations were carried out using a JEM-1011 (JEOL) transmission electron microscope at an accelerating voltage of 100 kV. High-resolution TEM images were obtained by using a TEM (Tecnai G2 F30 S-Twin, Philips-FEI, Netherlands) at an acceleration voltage of 300 kV. Samples for TEM observations were prepared by drop-casting of nanocrystals dispersed in hexane onto carbon film-coated copper TEM grids. Lattice distances and fast Fourier transform (FFT) of HRTEM images were characterized using Digital Micrograph software. Ultraviolet-visible-near infrared (UV-vis-NIR) (250 nm-900 nm) absorption spectra of prepared samples were measured in a 1 cm quartz cuvette using U-4100 spectrophotometer (HITACHI). The X-ray diffraction (XRD) patterns of prepared samples were taken on X'Pert Pro MPD (PANalytical) with $\text{CuK}\alpha$ radiation ($\lambda = 1.542 \text{ \AA}$) at 45 kV and 40 mA. The nanocrystals dispersed in hexane were drop-cast on a glass substrate and allow to dry for 60 min. The patterns were collected in 2θ ranging from 20-80 degrees with a step increment of 0.02 degree and a scan speed of 0.5 s step^{-1} . The data was analyzed using

a X'Pert HighScore Plus software and all the spectra were baseline corrected with respect to the spectrum of the amorphous glass background. Raman spectra of copper sulfide nanocrystals were recorded using inVia microscopic spectrometer (Renishaw). Data were obtained at $\lambda = 532$ nm with a 50 \times objective using a nominal power of 0.25 mW and integration time of 120 s.

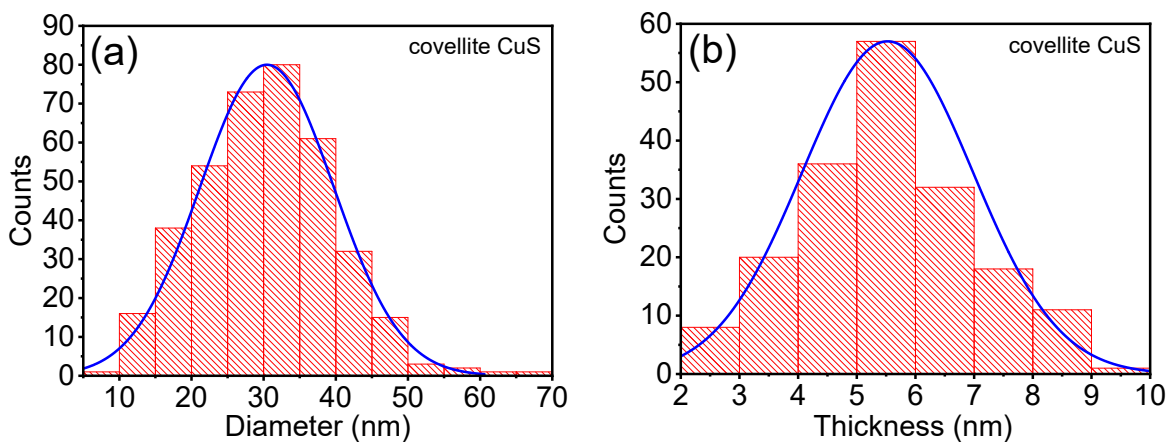


Figure S1. (a) Diameter- and (b) thickness-distribution histogram of covellite CuS nanodisks. Diameter: (30.4 ± 9.3) nm, thickness: (5.5 ± 1.4) nm.

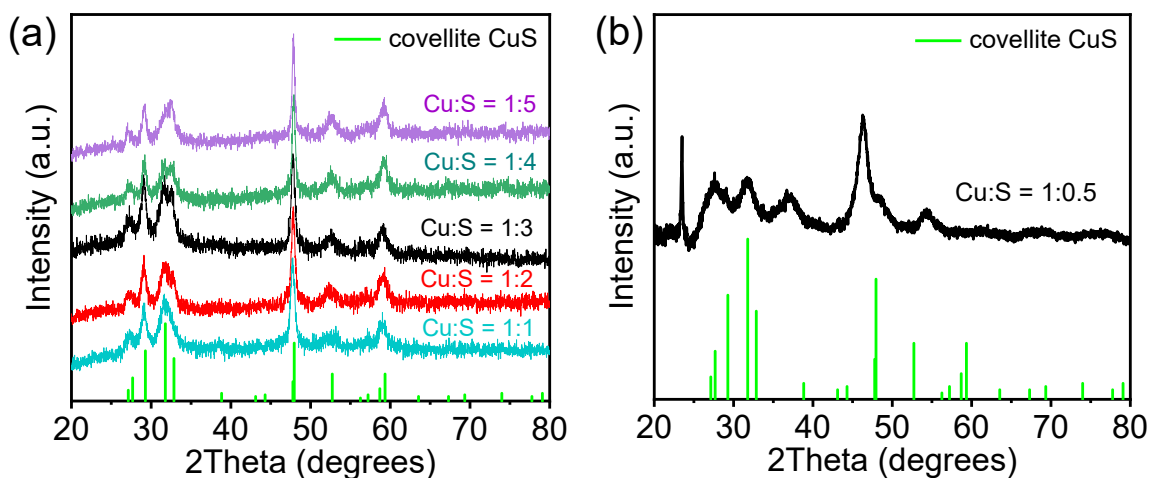


Figure S2. XRD patterns of covellite CuS nanodisks prepared by (a) tuning the Cu/S molar ratio from 1:1 to 1:5 and (b) Cu/S molar ratio of 1:0.5. Note: The CuS nanodisks prepared from Cu/S molar ratio of 1:3 were used for the phase transition in present study.

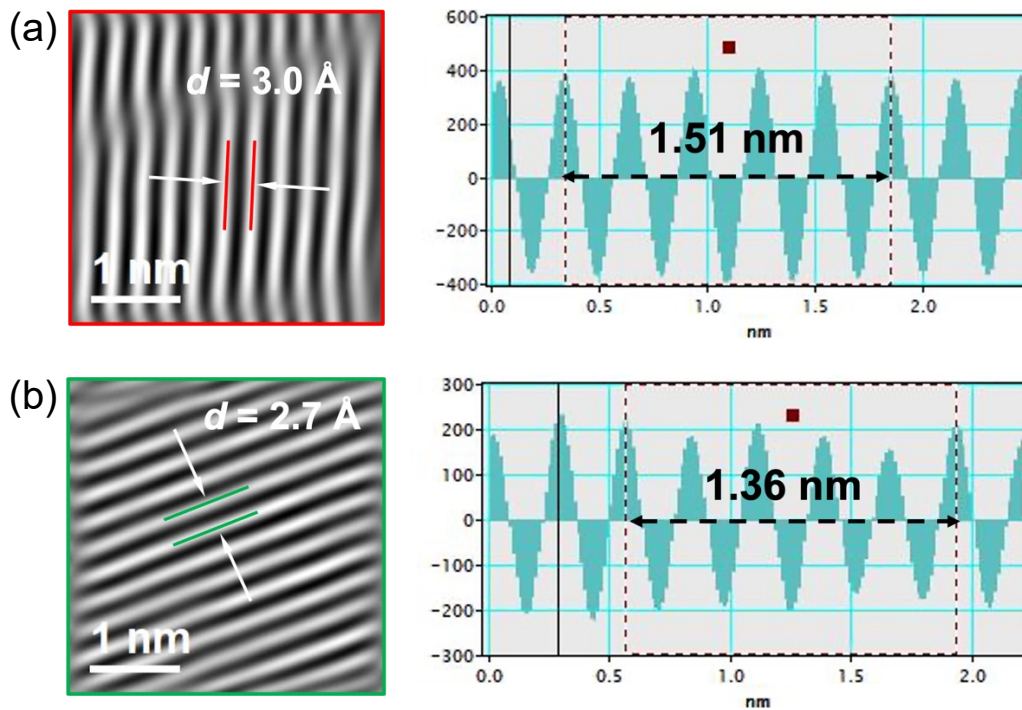


Figure S3. *inverse*-FFT pattern and according interplanar spacing of (a) (1 0 2) plane and (b) (0 0 6) plane of covellite CuS nanodisks.

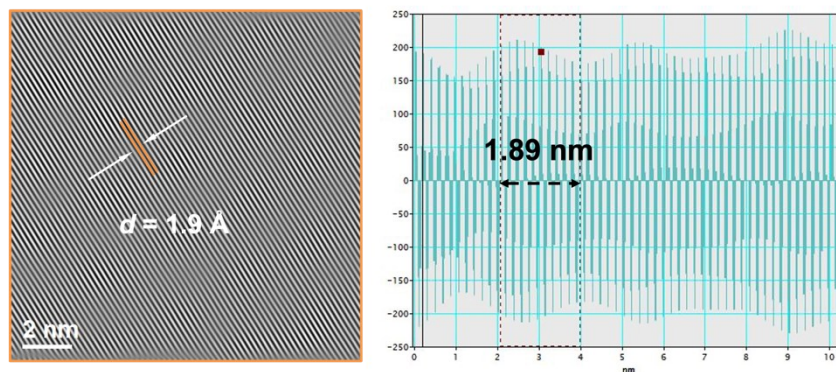


Figure S4. *inverse*-FFT pattern and according interplanar spacing of (1 1 0) plane of covellite CuS nanodisks.

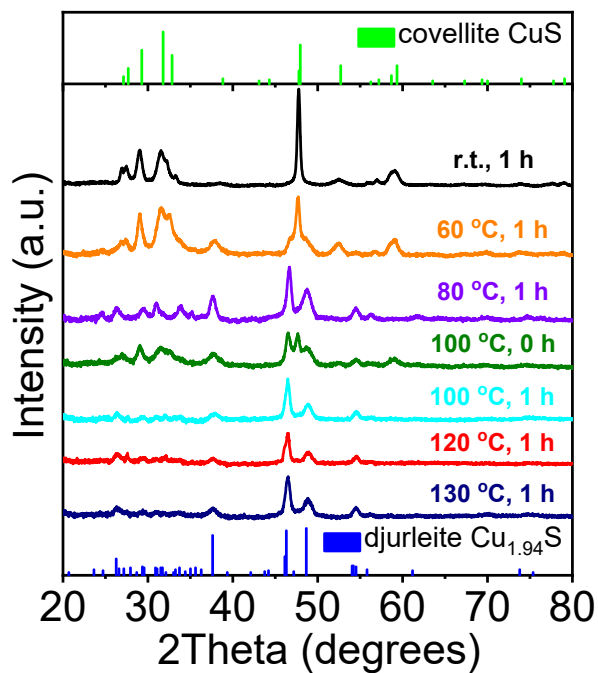


Figure S5. XRD patterns of covellite CuS nanodisks reduced by 1-DDT molecules at different temperatures.

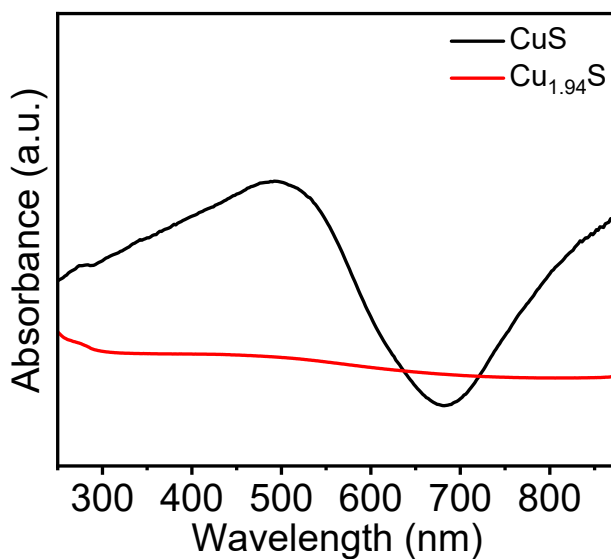


Figure S6. UV-vis-NIR absorption spectra of covellite CuS nanodisks and djurleite $\text{Cu}_{1.94}\text{S}$ nanodisks dispersed in hexane.

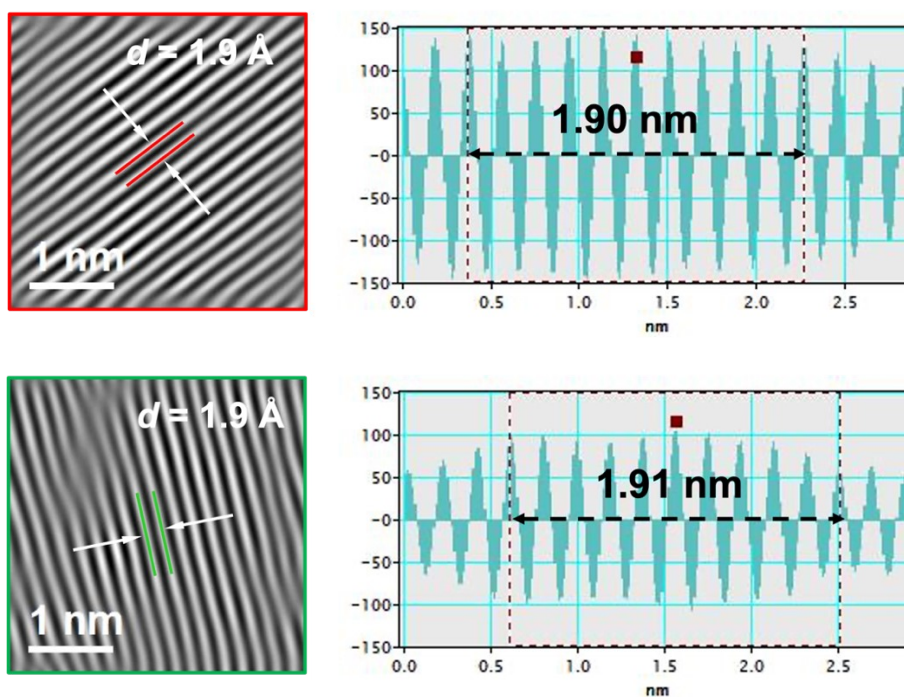


Figure S7. *inverse*-FFT patterns and according interplanar spacings of (12 0 4) planes of djurleite $\text{Cu}_{1.94}\text{S}$ nanodisks.

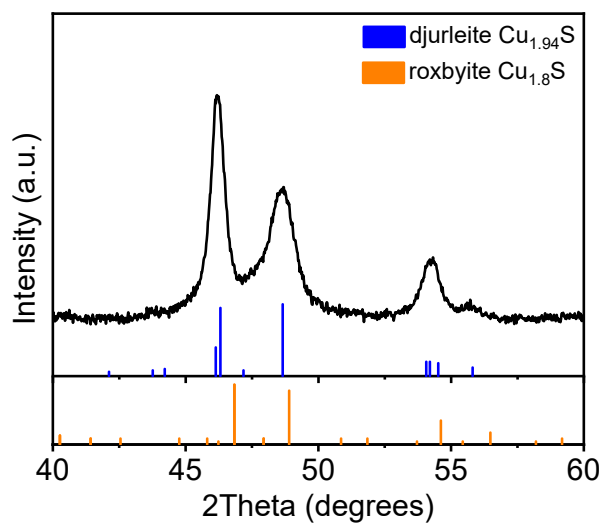


Figure S8. Enlarged XRD pattern of djurleite $\text{Cu}_{1.94}\text{S}$ nanodisks in Figure 2g.

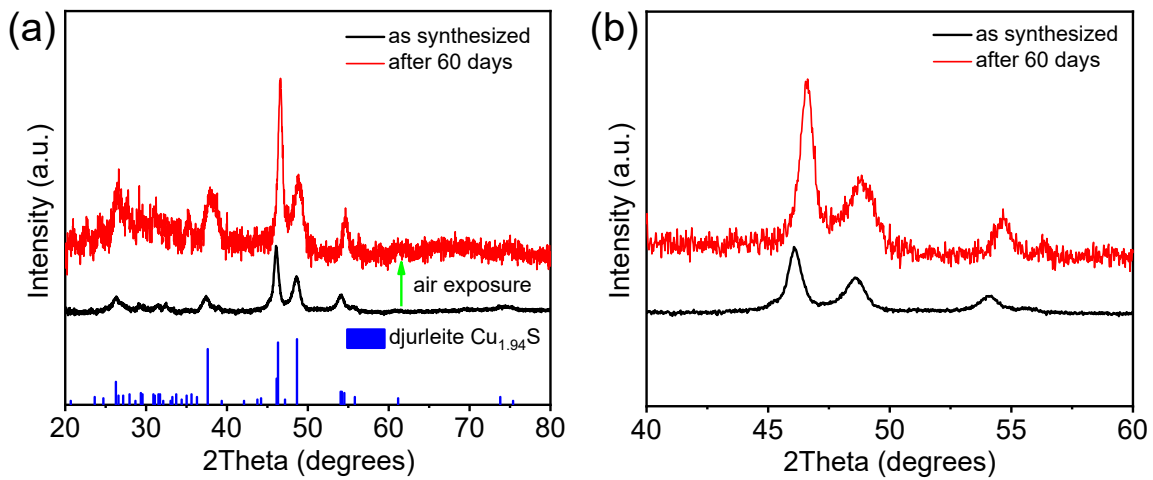


Figure S9. (a) XRD pattern and (b) enlarged XRD pattern of djurleite $\text{Cu}_{1.94}\text{S}$ nanodisks before and after 60 days air exposure.

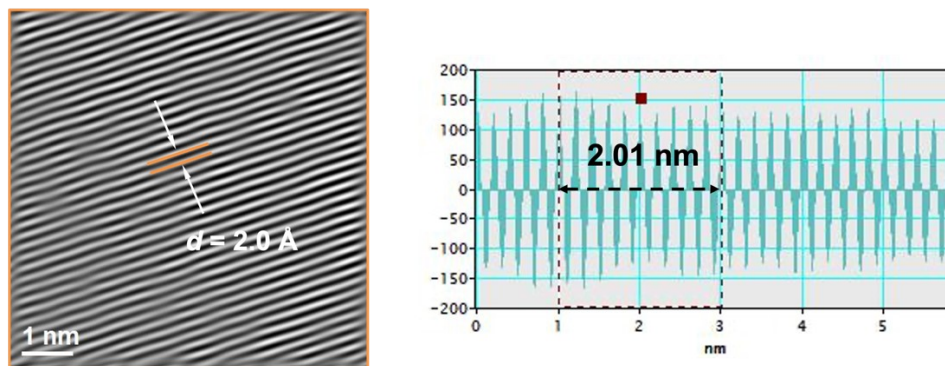


Figure S10. *inverse*-FFT pattern and according interplanar spacing of (0 8 0) plane of djurleite $\text{Cu}_{1.94}\text{S}$ nanodisk.

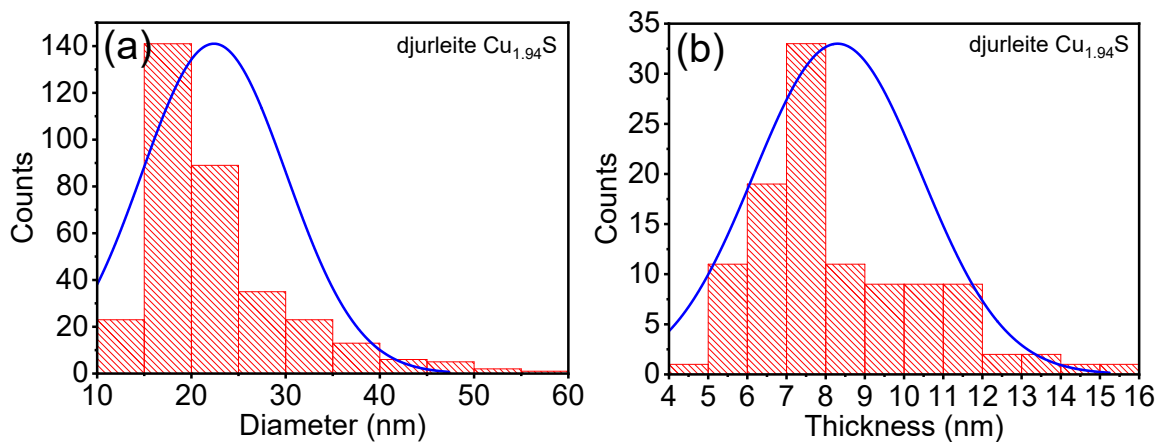


Figure S11. (a) Diameter- and (b) thickness-distribution histogram of djurleite $\text{Cu}_{1.94}\text{S}$ nanodisks. Diameter: (22.4 ± 7.7) nm, thickness: (8.3 ± 2.1) nm.

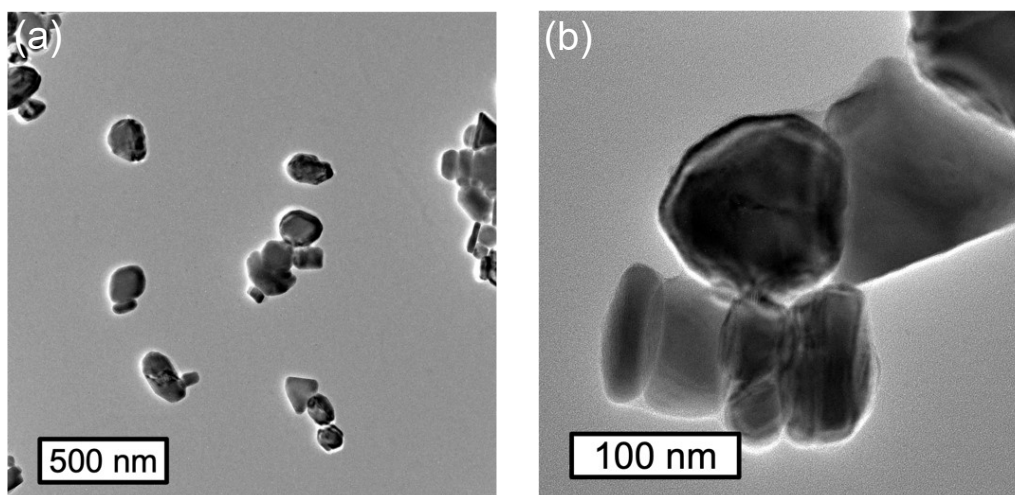


Figure S12. (a) TEM image and (b) HRTEM image of digenite $\text{Cu}_{1.8}\text{S}$ nanocrystals prepared by the thermal treatment of covellite CuS nanodisks in the presence of OAm molecules.

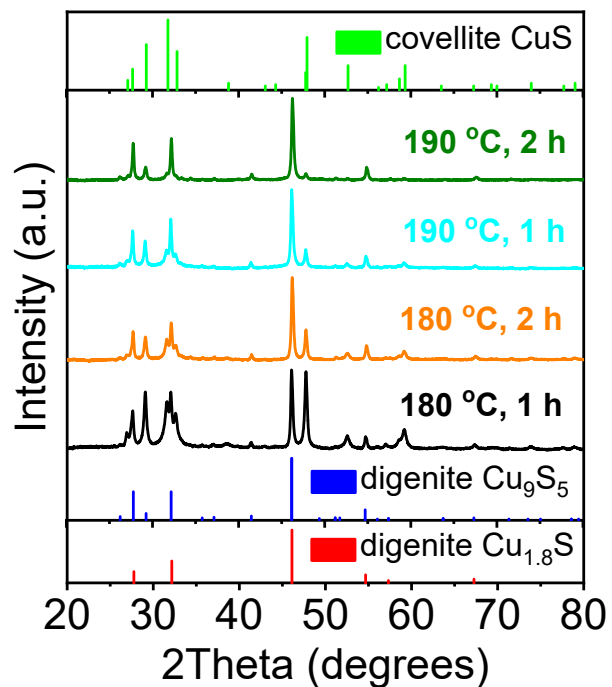


Figure S13. XRD patterns of covellite CuS nanodisks reduced by OAm molecules at 180 °C and 190 °C for 1 h and 2 h. Lower reduction temperature is set for understanding the morphology evolution during the phase transition process.

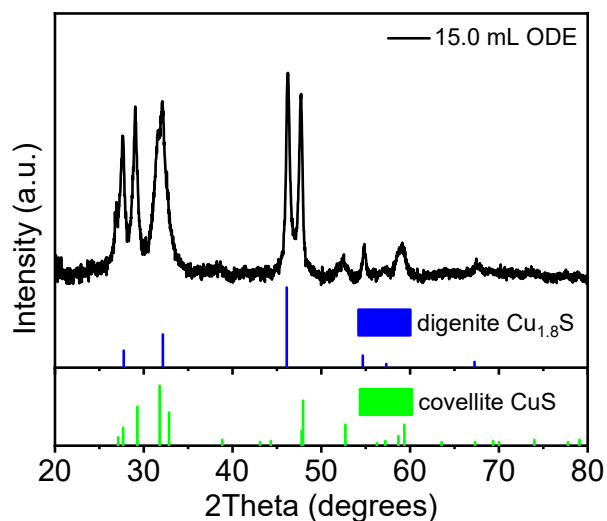


Figure S14. XRD pattern of covellite CuS nanodisks reduced by ODE at 200 °C for 1 h.

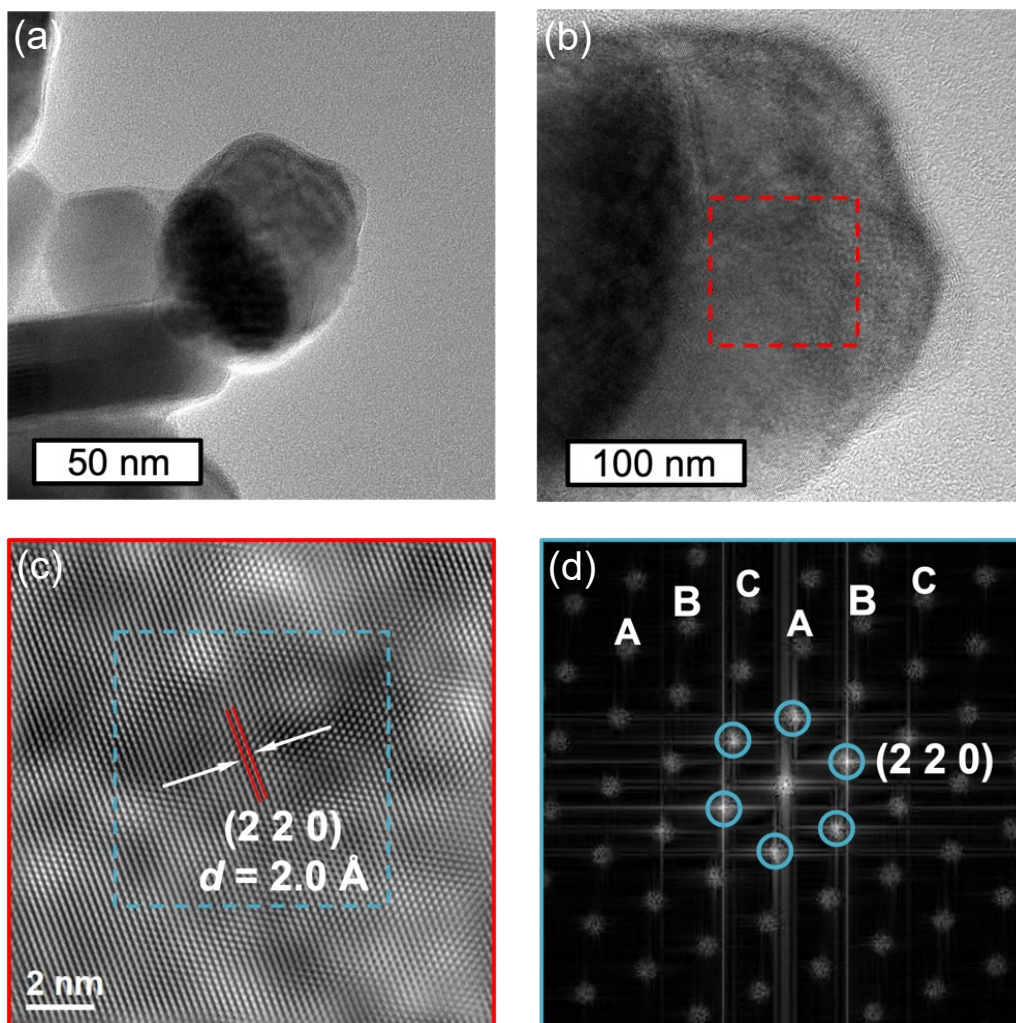


Figure S15. (a, b) (HR)TEM images, and according (c) *inverse*-FFT pattern and (d) FFT pattern of ccp digenite Cu_{1.8}S nanocrystals.

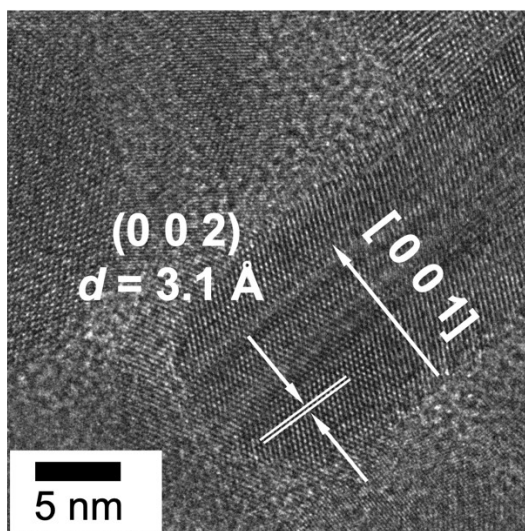


Figure S16. HRTEM image of wurtzite ZnS nanodisks.

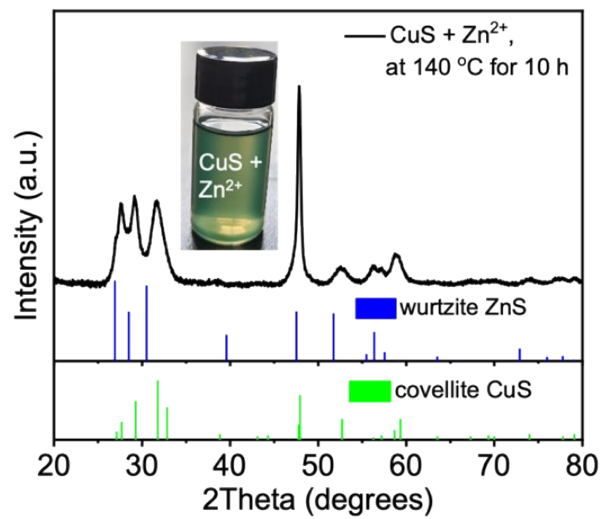


Figure S17. XRD pattern of CE product (greenish dispersion) by a direct reaction of covellite CuS nanodisks with Zn²⁺ at 140 °C for 10 h.

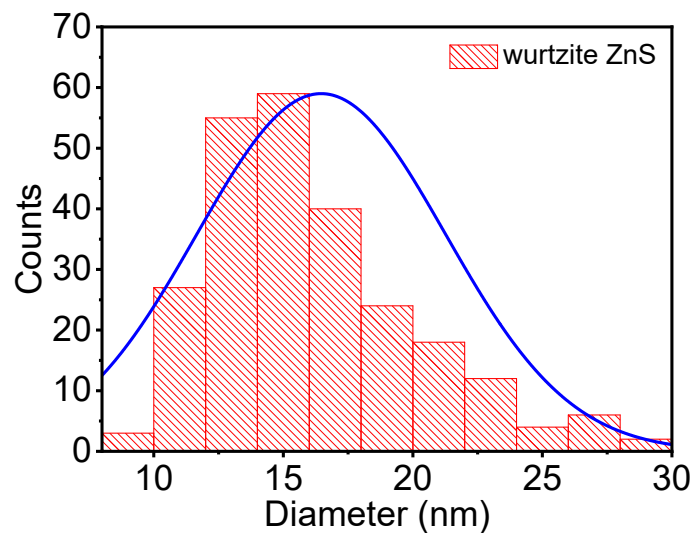


Figure S18. Diameter-distribution histogram of wurtzite ZnS nanodisks. Diameter: (16.5 ± 4.8) nm.

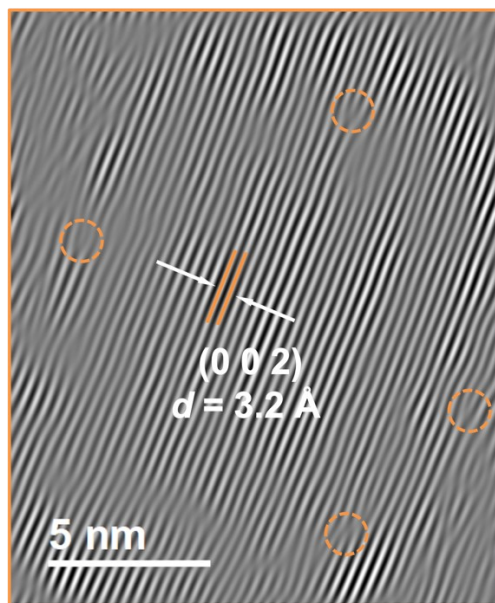


Figure S19. *inverse*-FFT pattern of wurtzite ZnS nanodisks taken from the region marked by an orange dashed rectangle in Figure 4b. The dashed orange circles indicate the existence of edge dislocations.

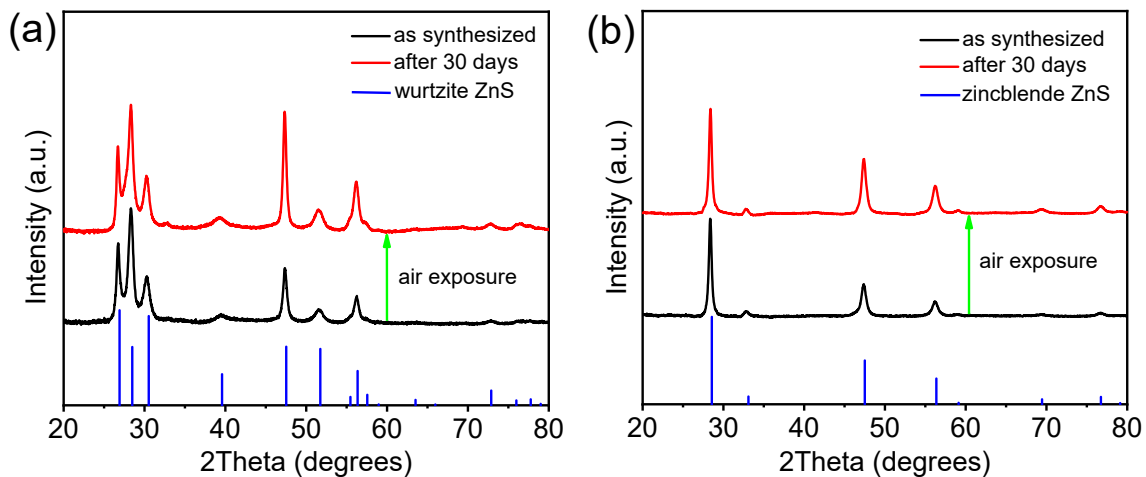


Figure S20. XRD patterns of (a) wurtzite ZnS nanodisks and (b) zincblende ZnS nanocrystals before and after 30 days air exposure.

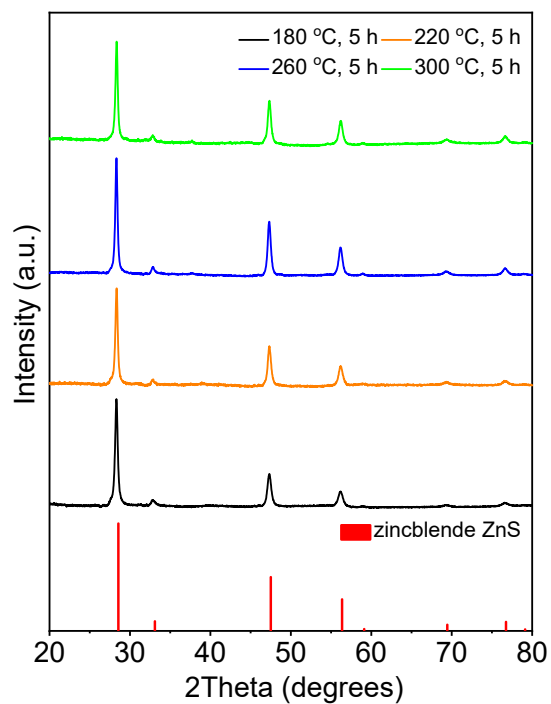


Figure S21. XRD patterns of zincblende ZnS NCs under thermal heating at different temperatures in the presence of OAm molecules and ODE molecules.

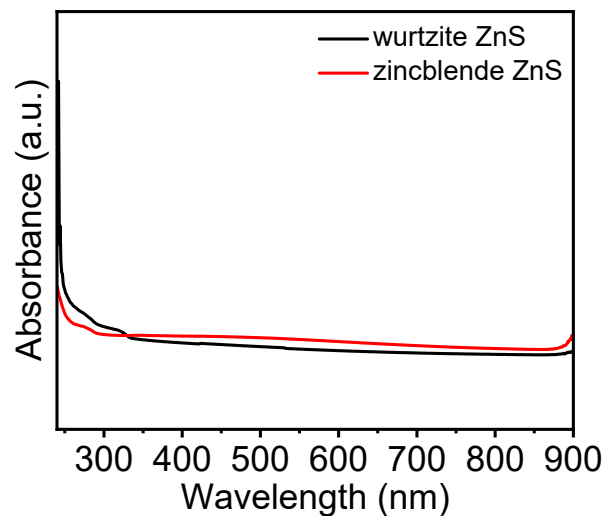


Figure S22. UV-vis-NIR absorption spectra of wurtzite ZnS nanodisks and zincblende ZnS nanocrystals dispersed in hexane.

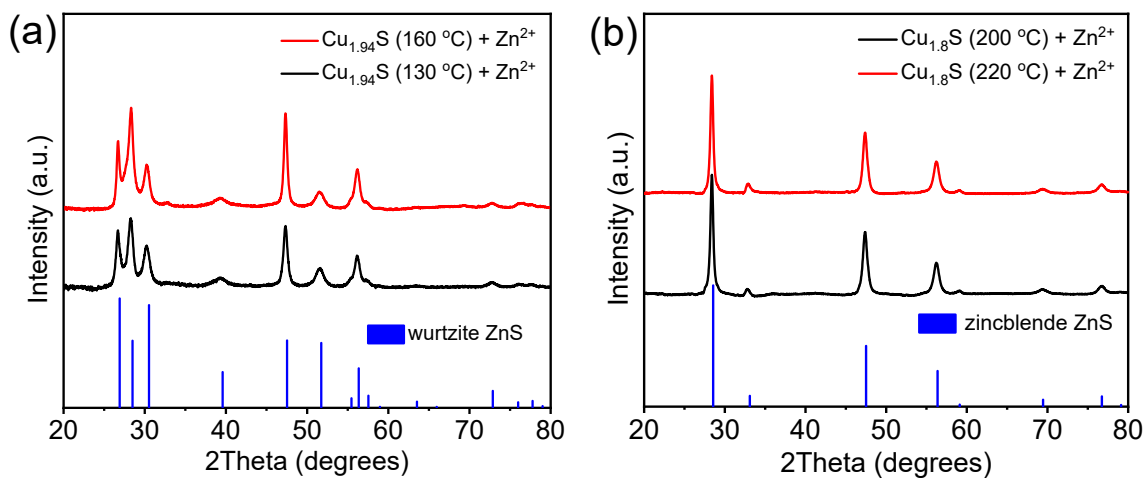


Figure S23. XRD patterns of (a) wurtzite ZnS and (b) zincblende ZnS from the CE reaction of different sized template nanocrystals. Note: The particle size of djurleite $\text{Cu}_{1.94}\text{S}$ nanodisks and digenite $\text{Cu}_{1.8}\text{S}$ nanocrystals can be tuned by the reduction of covellite CuS nanodisks at different temperatures.

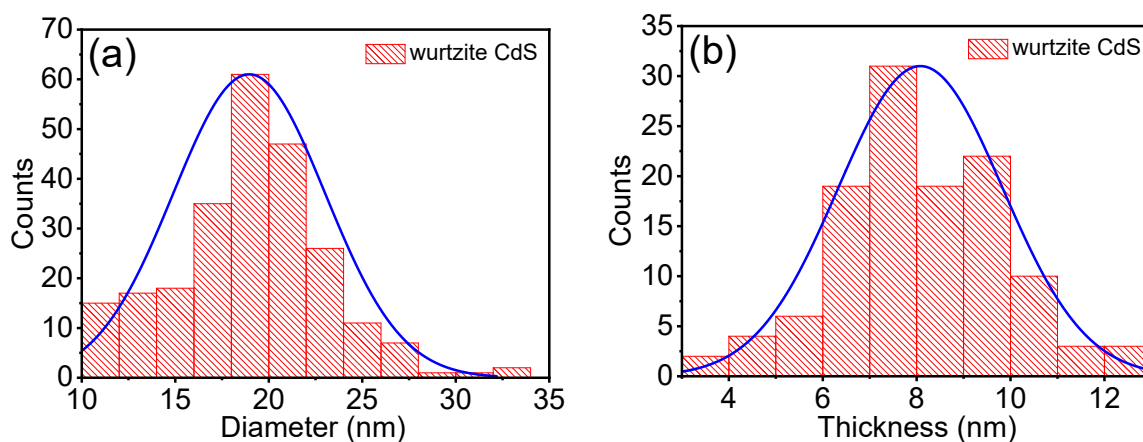


Figure S24. (a) Diameter- and (b) thickness-distribution histogram of wurtzite CdS nanodisks. Diameter: (18.9 ± 4.1) nm, thickness: (8.1 ± 1.7) nm.

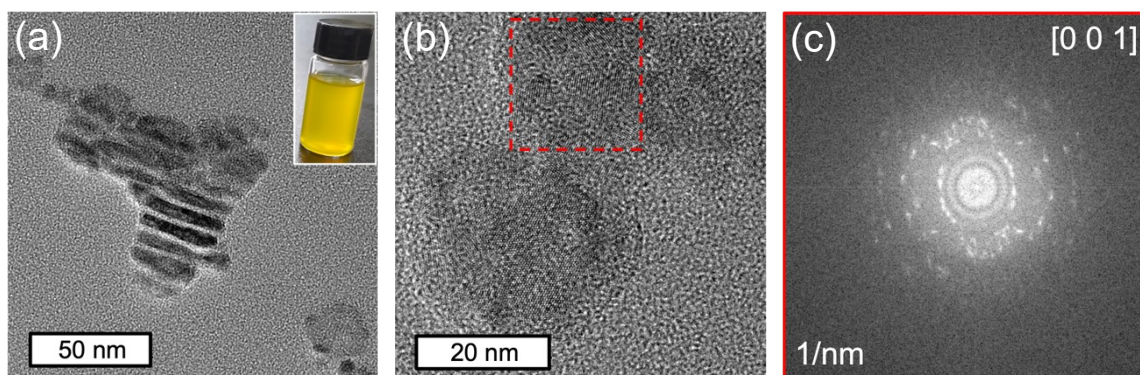


Figure S25. (a, b) (HR)TEM images and (c) FFT pattern of wurtzite CdS nanodisks by a direct reaction of covellite CuS nanodisks with Cd^{2+} at 140°C for 10 h. Inset: digital photograph of resulting CdS nanodisks dispersed in hexane.

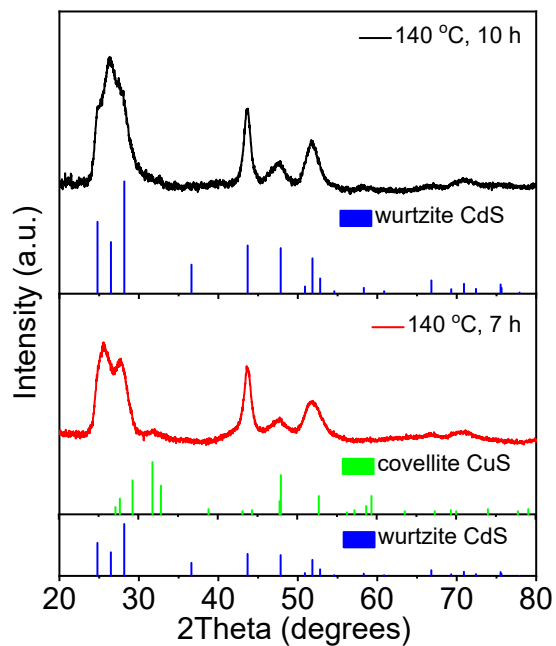


Figure S26. XRD patterns of CE product by a direct reaction of covellite CuS nanodisks with Cd^{2+} at 140 °C for 7 h and 10 h.

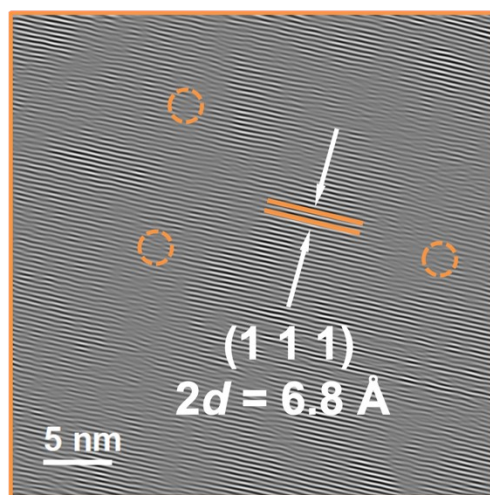


Figure S27. *inverse*-FFT pattern of zincblende CdS nanocrystals taken from the region marked by an orange dashed square in Figure 5e. The dashed orange circles indicate the existence of edge dislocations.

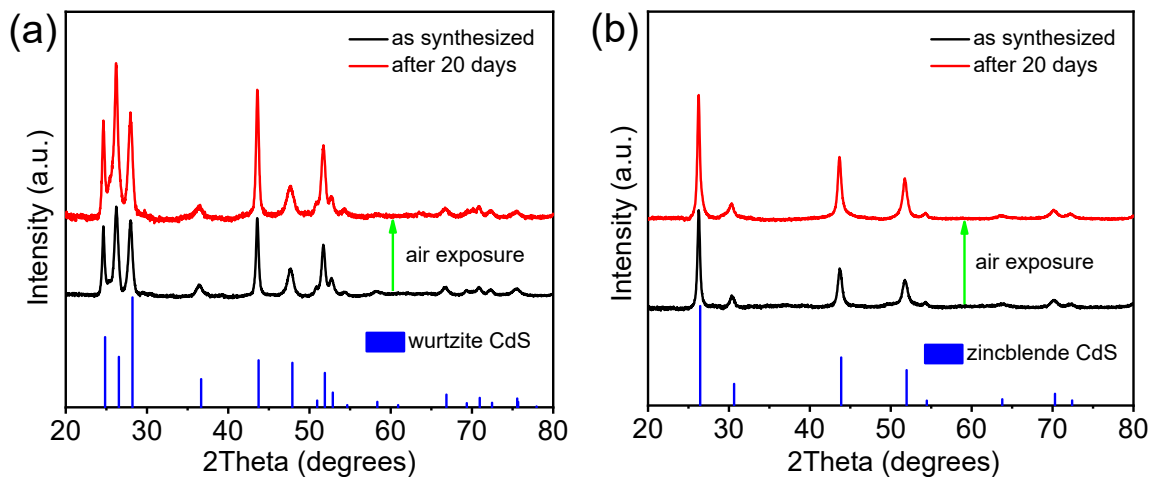


Figure S28. XRD patterns of (a) wurtzite CdS nanodisks and (b) zincblende CdS nanocrystals before and after 20 days air exposure.

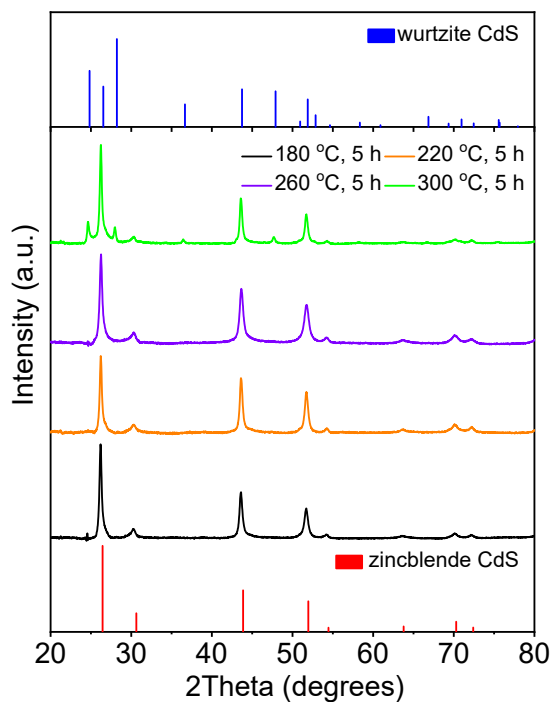


Figure S29. XRD patterns of zincblende CdS nanocrystals under thermal heating at different temperatures in the presence of OAm molecules and ODE molecules.

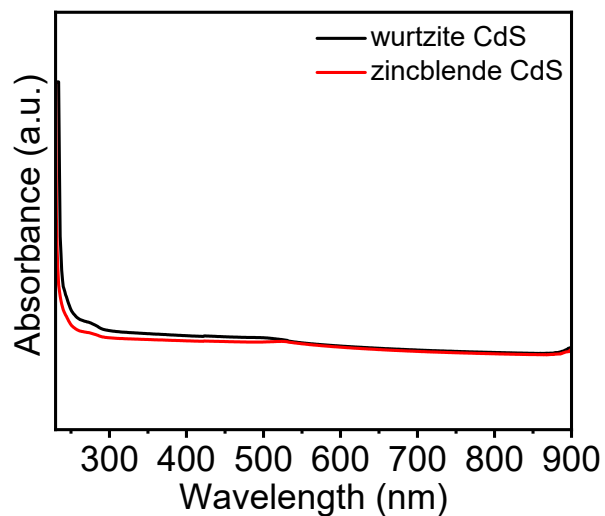


Figure S30. UV-vis-NIR absorption spectra of wurtzite CdS nanodisks and zincblende CdS nanocrystals dispersed in hexane.

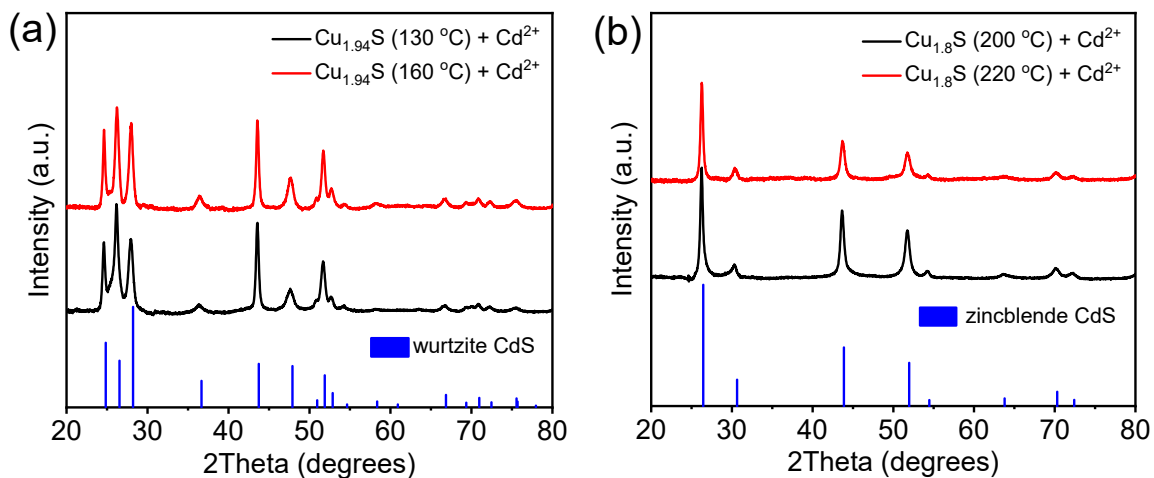


Figure S31. XRD patterns of (a) wurtzite CdS and (b) zincblende CdS from the CE reaction of different sized djurleite $\text{Cu}_{1.94}\text{S}$ nanodisks and digenite $\text{Cu}_{1.8}\text{S}$ nanocrystals.

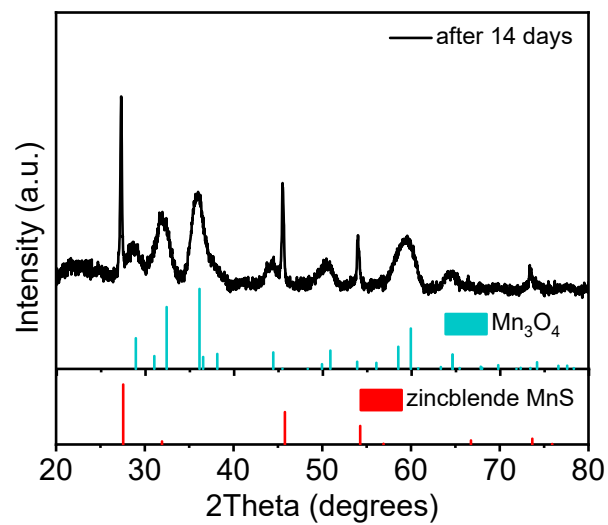


Figure S32. XRD pattern of zincblende MnS nanocrystals after 14 days air exposure.

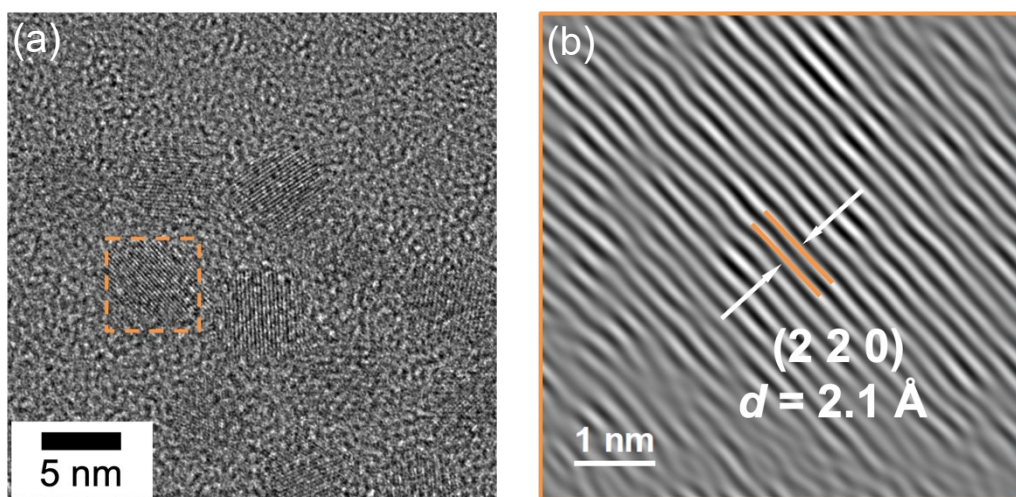


Figure S33. (a) HRTEM image and (b) according *inverse*-FFT pattern of dotted nanocrystals in Figure 6c. The interplanar spacing of 2.1 Å is assigned to (2 2 0) plane of Mn₃O₄.

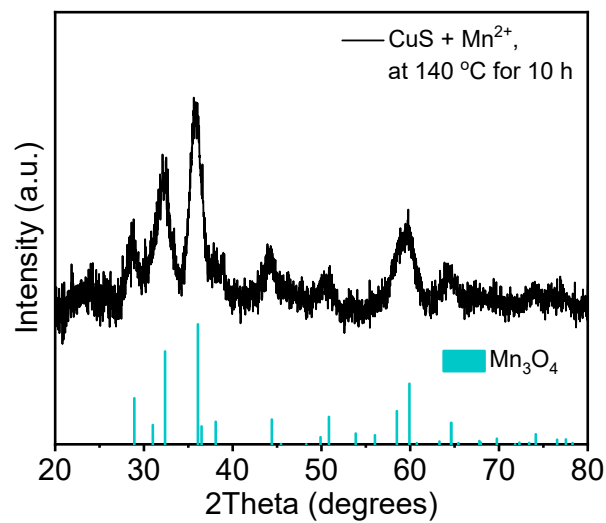


Figure S34. XRD pattern of CE product by a direct reaction of covellite CuS nanodisks with Mn^{2+} at 140 °C for 10 h. The oxygen element is probably from the impurities and residual O_2 in OAm, ODE, and TOP.

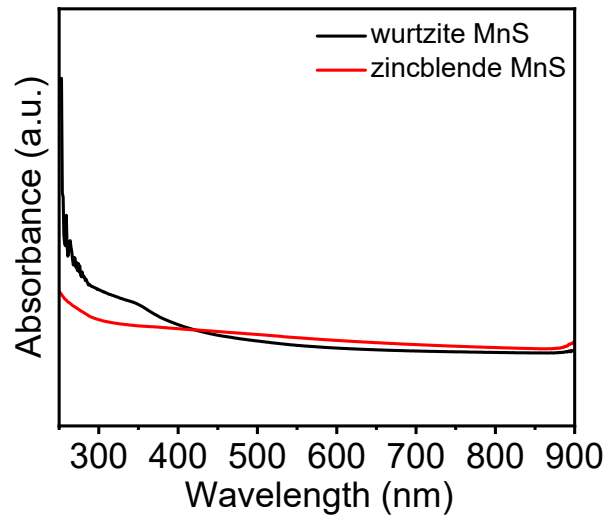


Figure S35. UV-vis-NIR absorption spectra of wurtzite and zincblende MnS nanocrystals dispersed in hexane.

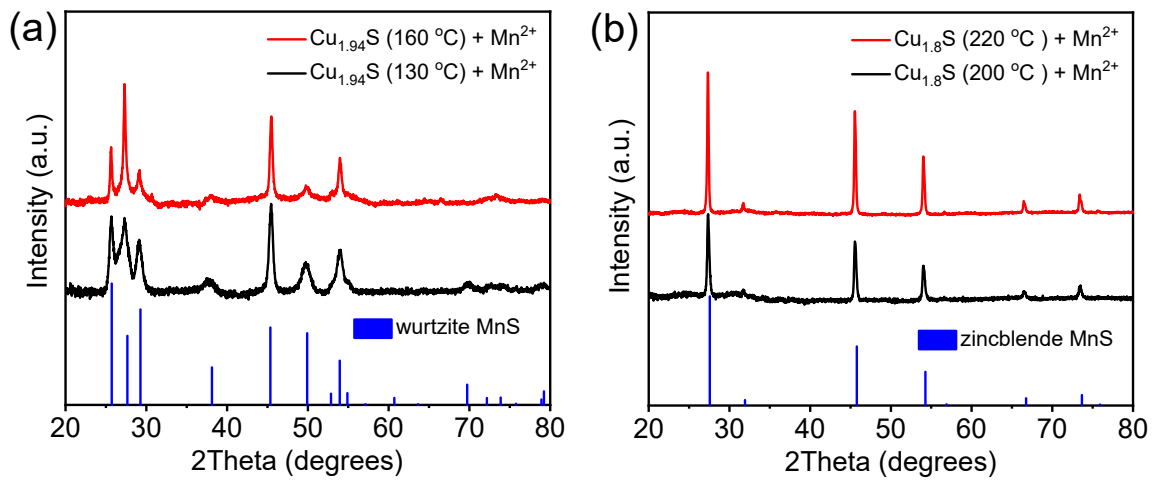


Figure S36. XRD patterns of (a) wurtzite MnS and (b) zincblende MnS from the CE reaction of different sized djurleite Cu_{1.94}S nanodisks and digenite Cu_{1.8}S nanocrystals.